Classical Molecular Dynamics Study of Small-Chain Carboxylic Acid Aerosol Particles

Antoine Roose, Céline Toubin, Sébastien Dusanter, Véronique Riffault, Denis Duflot

ACS EARTH AND SPACE CHEMISTRY

Article

Cite This: ACS Earth Space Chem. 2019, 3, 380−389

http://pubs.acs.org/journal/aesccq

Classical Molecular Dynamics Study of Small-Chain Carboxylic Acid Aerosol Particles

Antoine Roose,[†,‡] Céline Toubin,[†] Sébastien Dusanter,[‡] Véronique Riffault,[‡] and Denis Duflot*[,†]

[†]Université de Lille, CNRS, UMR 8523 - PhLAM - Physique des Lasers Atomes et Molécules, F-59000 Lille, France

[‡]Département Sciences de l'Atmosphère et Génie de l'Environnement (SAGE), IMT Lille Douai, Université de Lille, F-59000 Lille, France

Supporting Information

ABSTRACT: The growth of small valeric (pentanoic) and glutaric (pentanedioic) acid aerosol particles from 20 to 500 molecules has been investigated at room temperature using classical molecular dynamics simulations. As a result of a higher propensity to form hydrogen bonds, glutaric acid aggregates are shown to be denser than their valeric counterpart. The addition of water molecules with water/acid ratios of 1:1 and 2:1 has then been studied in the case of the diacid. At a low water content, water primarily forms small islands on the surface. When the amount of water increases, it penetrates deeper into the aggregate but a significant fraction remains at the surface. A Connolly surface analysis reveals that the surface is mostly covered by hydrogen atoms from CH_2 groups, with acidic hydrogens being saturated and not available at the surface, for both dry and wet particles. These atomic distributions could impact the reactivity of such particles with gas-phase oxidants and the uptake of trace gases.

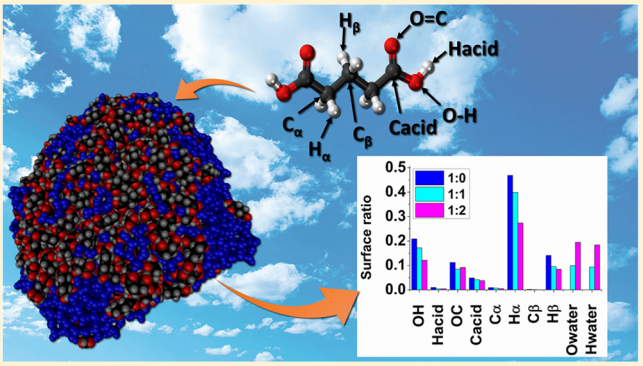

KEYWORDS: *glutaric acid, valeric acid, classical molecular dynamics, aerosol, atmosphere*

INTRODUCTION

It is well-known that atmospheric aerosols contain a significant part of carbonaceous compounds, either elemental (black carbon and fresh soot), organic, or a mixture of both types (brown carbon).[1] They can be primarily emitted from either biomass burning or other anthropogenic sources or formed via the oxidation of gaseous precursors. In addition to their direct effect on the radiative balance of the Earth,[2] they can also act as cloud condensation nuclei (CCN)[3] onto which water will condense to form cloud droplets. In this context, a better understanding of their formation processes and interaction with water is fundamental.

Carboxylic acids are ubiquitous in the atmosphere and constitute one of the most abundant groups of species among organic compounds as oxidation end products.[4,5] These acids have been observed in both the gas and particulate phases, with low-molecular-weight compounds, such as formic and acetic acids, being mainly observed in the gas phase,[6] and higher molecular weight compounds, such as dicarboxylic acids, partitioning predominantly to the particulate phase.[7] Small-chain fatty acids (mono- and dicarboxylic) have for example been detected in various areas,[8,7−10] including valeric acid (VA) and glutaric acid (GA). For example, in the north of France, measurements at an urban background in Douai[9] and an industrialized coastal site in Dunkirk[10] gave concentrations of only a few nanograms per meter cubed on a daily average with no clear seasonal trend.

To better understand the formation of secondary organic aerosols (SOAs) and the impact of environmental conditions, such as relative humidity (RH) and temperature, on their atmospheric fate, simulation tools are paramount. Several molecular dynamics (MD) studies have focused previously on organic aerosols, with some of them specifically on carboxylic acid aerosols. Ma et al.[11] have studied the behavior of inverted micelles of a dicarboxylic acid (C_3−C_9 and branched C_9) layer on a droplet of water at 300 K and observed the formation of two separate phases, except for malonic acid (C_3), which dissolves in water. Water nucleation was also investigated by MD simulations on small dicarboxylic acid aggregates[12,13] as well as formic,[14] acetic, and propionic acid aggregates[15] in the 100−250 K temperature range. These authors have highlighted that pressure does not have a strong influence, in contrast to the temperature and RH. For the highest temperature range ($200 < T < 250$ K), mixed water−acid droplets were formed, while water islands were observed at lower temperatures. More recently, the same kind of study has been performed on mixed formic and acetic acid aggregates.[16] These simulations have shown that the interaction between both acids has no influence

Received: November 6, 2018
Revised: February 11, 2019
Accepted: February 12, 2019
Published: February 12, 2019

DOI: 10.1021/acsearthspacechem.8b00172
ACS Earth Space Chem. 2019, 3, 380−389

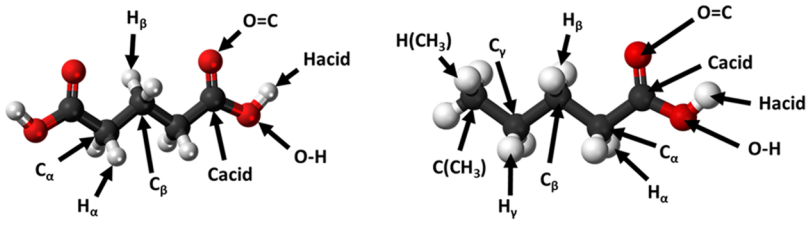

Figure 1. Labeling of atoms and functional groups in both molecules.

and the overall behavior is similar to what was found for the pure organic aggregates.

These MD studies could be used to provide a better understanding of observations made in laboratory experiments, such as studies focusing on the uptake of trace gases on atmospheric aerosols. Indeed, some experiments carried out by Taketani et al.[17] and Lakey et al.[18] on dicarboxylic acid particles have highlighted some trends for the hydroperoxy radical (HO_2) uptake, which depends upon RH. Humidity can increase the uptake because it can enhance the diffusivity of gaseous compounds in the bulk.[19] On the contrary, Lakey et al.[18] have also estimated that, for some organic aerosols, such as humic acids, the increase of RH can finally lead to the formation of a micelle, which creates a diffusion barrier and, thus, decreases the uptake. Studying the structure of organic aerosols by MD can lead to the prediction of such effects.

The goal of the present paper is to study the properties of small organic aerosols, formed of GA molecules ($C_5H_8O_4$), and to perform a comparison to its monoacid counterpart, i.e., VA ($C_5H_{10}O_2$). In addition, this study investigates the adsorption of water molecules on the glutaric aerosol surface. Indeed, as a result of the size of the molecules, quantum calculations can only be considered for small clusters[20] and the use of classical MD techniques is mandatory.

COMPUTATIONAL DETAILS

Aerosols of pure VA, pure GA, and wetted GA were generated by classical MD simulations with the GROMACS program package (version 5.0.7).[21]

The geometries of isolated VA and GA molecules (Figure 1) were both optimized quantum mechanically at the M06-2X/6-311++G** and MP2/6-31+G** levels,[22−24] respectively, using the Gaussian 09 quantum package.[25] Topology files were generated with the Antechamber program[26] using the parameters from the AMBER GAFF force field[27] (see the Supporting Information). RESP charges[28−30] for GA have been computed at the MP2/6-31+G** level, while for VA, AM1-BCC charges were used.[31] Water was described with the SPC/E model.[32]

The simulations have been performed in the *NVT* canonical ensemble after an energy minimization with the steepest descent algorithm. The temperature was kept fixed at 300 K with the velocity rescale algorithm and a coupling time of 0.1 ps.[33] The cubic box was set to a width of 30 nm. Dry aerosols were formed from the aggregation of 20, 50, 100, 200, and 500 molecules of carboxylic acids, randomly placed inside the box. The *NVT* simulation was performed with a time step of 2 fs until stabilization of the total energy. The total simulation time was 60 ns for dry aggregates and 40 ns for wet aggregates, except for the 500 wet case, where the simulations were prolonged for 50 ns. All calculated properties appear to be converged after 30 ns. Finally, 2 ns of production was used for the analysis. Molecules were kept rigid thanks to the LINCS algorithm,[34] where only the angles are free to move, except for water, constrained in the SPC/E geometry. The intermolecular interactions (Coulomb and Lennard−Jones) have been cut beyond 1.2 nm. To take into account the long-range electrostatic interaction, the particle mesh Ewald (PME) method has been used,[35] with a Fourier spacing of 0.12 nm.

Once the aggregate is formed, its angular momentum starts to increase because there is no collision. To remove this artificial motion that leads to the breaking of the aggregate, the center of mass rotation was disabled for 10 ns, with the periodicity of the box and the constraint on the bonds (LINCS algorithm) also being removed during this period. The time step used was decreased from 2 to 0.5 fs. The long-range intermolecular interaction has also been removed, and the cutoff radii for the Lennard−Jones and Coulombic interactions were set to 6 nm to take into account all of the interatomic interactions. Once the aggregate becomes stabilized, the rotation is reactivated and the run is prolonged.

Wetted aggregates have been generated for 1:1 and 1:2 GA/water ratios. The corresponding amount of water molecules was added randomly on the previously obtained dry GA aggregates. It should be noted that only neutral molecules were considered in the present work, even though deprotonated molecules could also be found in atmospheric particles.[36]

Finally, a Connolly surface analysis[37] has been performed using a probing sphere of 0.2 nm with a precision of 500 dots per sphere using the method described by Eisenhaber et al.[38] Note that the Connolly surface corresponds to the contact between the sampling sphere and the van der Waals surface of the aerosol. This provides an estimate of the atomic distribution at the surface of the particle as well as its surface and volume (see Table 1).

RESULTS AND DISCUSSION

Geometries of Gas-Phase Acids. Before turning to the analysis of the particle phase, it is worth mentioning an important difference between GA and VA geometries in the gas phase (see Figure 1). Indeed, while isolated VA has a unique geometry of C_s symmetry, GA has three possible conformers (see the Supporting Information). The less stable conformer corresponds to a C_s symmetry similar to VA. The second conformer is stabilized by an intramolecular hydrogen bond between C═O oxygen and the opposite H_α hydrogen atom. At the MP2/6-31+G** level, this conformer is 1.64 kcal mol^{-1} lower in energy. Finally, the third conformation has a hydrogen bond between C═O oxygen and the opposite O−H hydrogen, making it more stable by 4.81 kcal mol^{-1} (MP2/6-31+G*). With a higher level of theory (MP2/aug-cc-pVTZ), the relative energies are not modified significantly (−0.94 and

DOI: 10.1021/acsearthspacechem.8b00172
ACS Earth Space Chem. 2019, 3, 380−389

Table 1. List of the Particle Surfaces and Volumes Given by the Connolly Surface Analysis and Corresponding Calculated Densities

N	surface (nm^2)	volume (nm^3)	density (g/cm^3)
		GA	
20	19.8	6.3	0.70
50	33.8	13.6	0.81
100	50.1	24.6	0.89
200	76.2	45.3	0.97
500	136.5	106.0	1.04
		VA	
20	23.0	6.8	0.50
50	41.7	14.9	0.57
100	63.9	27.4	0.62
200	109.0	49.0	0.66
500	173.0	116.2	0.73
		1:1 GA/Water	
20	32.9	8.4	0.60
50	40.1	16.0	0.78
100	58.6	28.7	0.87
500	151.8	121.7	1.02
		1:2 GA/Water	
20	29.2	8.6	0.65
50	47.8	18.5	0.76
500	171.0	137.3	1.02

-3.66 kcal mol^{-1}, respectively), as also happens for other dicarboxylic acids.[20] All conformers appear to have very similar RESP charges. However, in the aerosol phase, the intramolecular hydrogen bonds are broken to the benefit of intermolecular hydrogen bonds. For this reason, the RESP charges calculated for conformer 1 geometry were used in the MD simulations.

As detailed in the Supporting Information, the force-field parameters were validated by comparing the calculated density and lattice parameters of the bulk crystals to available experimental values.[39−41] The geometry and energy (see below) of the hydrogen bonds were also compared to experimental values as well as *ab initio* results obtained at the MP2/6-311++G(2d,2p) level with zero-point energy (ZPE) corrections.

Structure of VA and GA Aggregates. The snapshots of dry GA and VA aerosols, shown in panels a and b of Figure 2, do not exhibit noticeable differences, thus requiring the calculation of several observables to quantitatively differentiate the two acid aggregation properties.

Radial distribution functions (RDFs), $g(r)$, were obtained by computing the distance between the mass center of the molecule or a functional group and the mass center of the whole aggregate, fixed at $r = 0$ nm. RDFs have been calculated for the COOH group of both acids, the $(CH_2)_\beta$ carbon chain of GA, and the CH_3 tail of VA with respect to the aggregate mass center. Note that, for clarity, RDFs shown in Figure 3 are not normalized. For all studied sizes from 20 to 500 GA molecules, the two distributions exhibit well-correlated peaks, with the atoms being uniformly distributed in the volume of the aggregate. For VA, the behavior of $g(r)$ is rather similar. For smaller sizes (N = 20 and 50), the COOH functions are located close to the center of the aggregate. This is due to the creation of intermolecular hydrogen bonds between the COOH groups at the center. When the size increases, the COOH groups are still located in the particle bulk, while the CH_3 groups are becoming more abundant toward the surface.

The GA RDFs exhibit sharper oscillations than the VA RDFs as a result of the formation of hydrogen bonds on both sides of the chains, which provide additional structural features. This effect has also been observed for the orientation of the

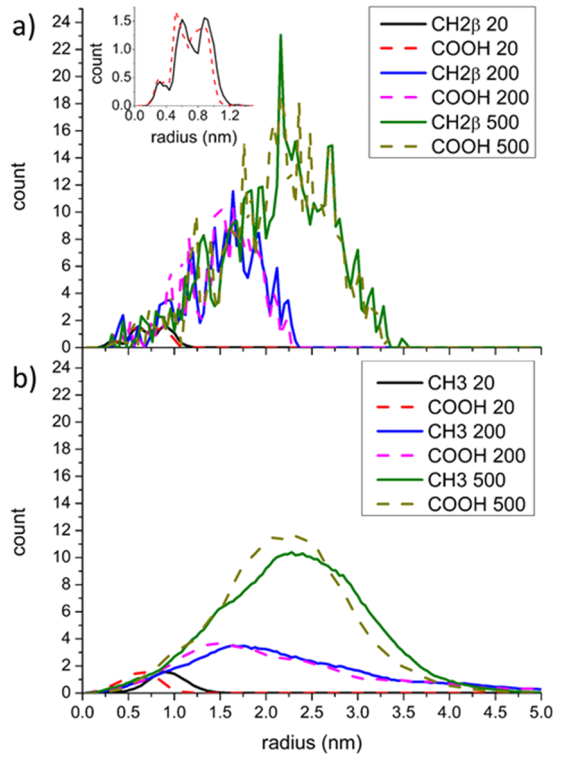

Figure 3. Mean number of specific atom groups as a function of the distance to the (a) GA and (b) VA aerosol centers of mass. The solid and dashed curves represent the distribution functions of the centers of mass of $CH_{2\beta}$ (GA) or CH_3 (VA) and COOH, respectively.

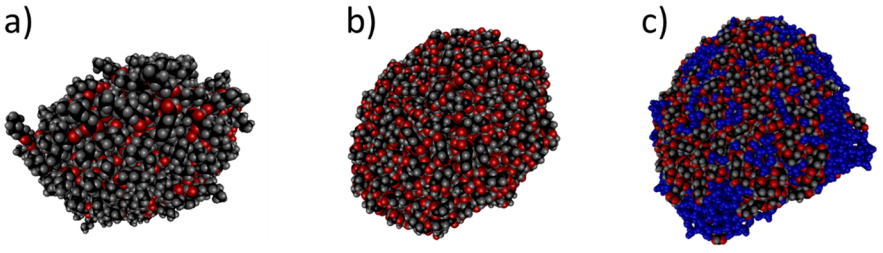

Figure 2. Snapshots of dry (a) VA and (b) GA aggregates containing 500 molecules and (c) 1:2 acid/water aggregate composed of 500 GA molecules.

DOI: 10.1021/acsearthspacechem.8b00172
ACS Earth Space Chem. 2019, 3, 380−389

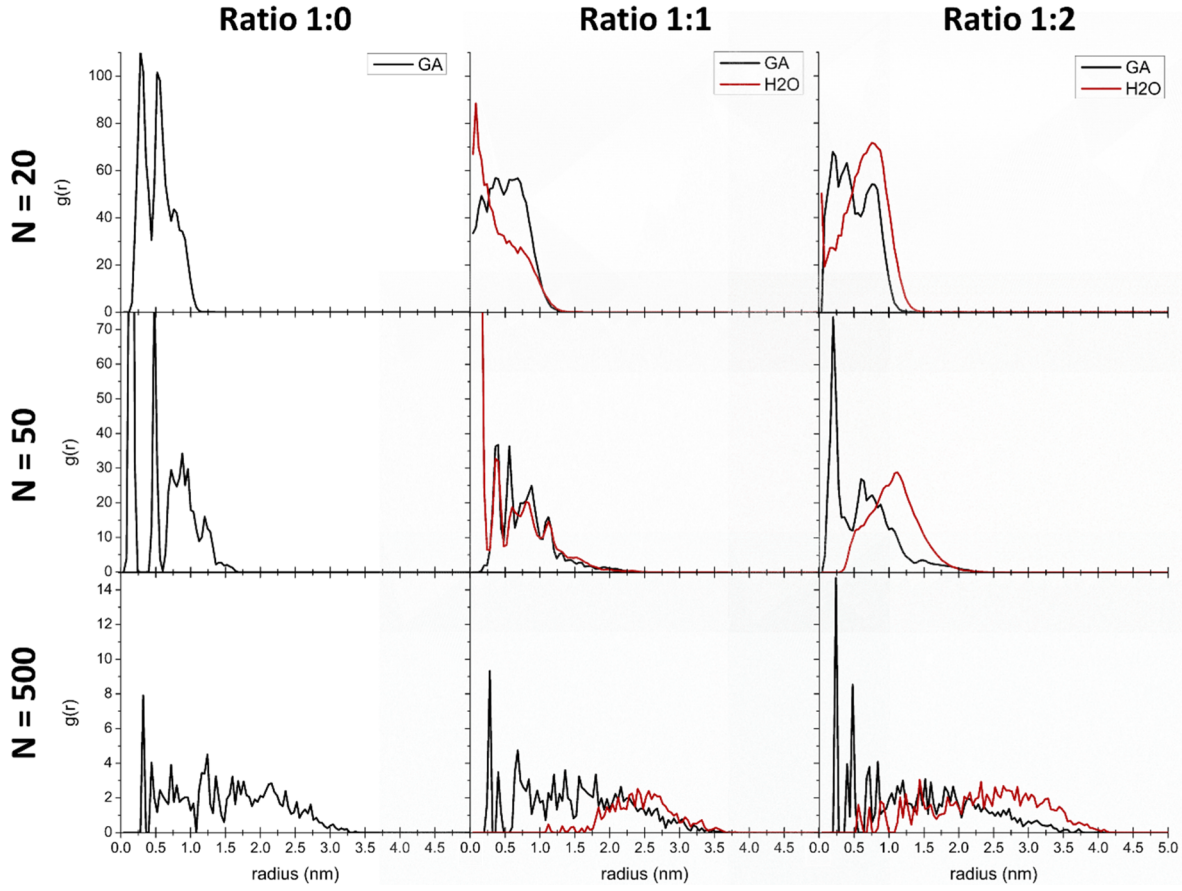

Figure 4. RDFs of (left) dry GA and (middle) 1:1 and (right) 1:2 ratios of GA/water aggregates. The black curve corresponds to the GA center of mass, and the red curve corresponds to the water center of mass.

chains (see the angle distributions presented as Supporting Information).

It is interesting to see how the organization of the chains in the aggregate is affected by the subsequent addition of water. In Figure 2c, a snapshot of the aggregate with 500 GA molecules and 1000 water molecules is shown as an example. In Figure 4, the RDFs of GA and water mass centers for both 1:1 and 1:2 ratios are compared to the RDF of the glutaric center of mass without water at the corresponding size. For the 1:1 ratio and N = 20, the water molecules are located at the center of the cluster, with the acid being repelled outside. At this size, water manages to diffuse between the acid molecules that are less strongly bonded than at larger sizes, as shown later. As the size becomes significant (N = 500) for the 1:1 ratio, most of the water molecules are at the upper edge (r > 2 nm). This is in line with the results of Radola et al.[15] for a N = 120 1:1 propionic acid/water cluster simulated at 250 K; at this water content, the acid aerosol is preserved at the center. It is possible that, for higher acid/water ratios, the acid would create a shell around a water droplet, as found in the propionic acid/water case studied by Radola et al.[15]

When the ratio is increased to 1:2 (Figure 4), the situation is somewhat different because, for small aggregates, the water molecules lie preferentially at the surface of the aggregate, whereas for N = 500, water molecules can also be found in the core of the particle. The larger number of molecules present at the surface tends to create a pseudo-pressure that pushes the water molecules toward the interior. It should be noted that simulations have been extended to 90 ns for both ratios and the largest sizes, N = 200 and 500, to make sure that the distributions are not dependent upon the sampling time, because the diffusion process requires a longer simulation time to be captured.[13] The diffusion of water through an organic core has also been observed by Zhang et al.[42] for a size of N = 120 acetic acid molecules and a 1:3 acid/water ratio at 260 K. For larger acid/water ratios (1:6 or 1:10) and fewer propionic acid molecules (N = 120), Radola et al.[15] showed that, at 250 K, water forms a liquid droplet at the center of the particle, with the acid molecules being repelled toward the edge of the particle. This behavior is consistent with our own results obtained with lower water coverage, longer chains, and larger aggregates, at room temperature.

Using these functions, it is possible to estimate the radius of the formed aggregate. For a homogeneous particle, this radius should be proportional to a power of the number of molecules N: $r(N) = r_0 N^{\alpha}$. Ideally, α should be equal to $^1/_3$ if we assume that the aggregate has a spherical shape. Figure 5 depicts the radius of dry GA and VA particles as a function of N together with a fit of the above function. The radius was obtained by taking the distance corresponding to 5% of the maximum value of the non-normalized RDF. The radii deduced for dry aggregates of both acids appear to closely follow this law, because α = 0.306 and 0.379 for GA and VA, respectively. Interestingly, r_0(GA) = 0.48 nm and r_0(VA) = 0.38 nm, which roughly correspond to half of the length of each isolated molecule (0.37 nm for GA and 0.39 nm for VA). Thus, both acid aggregates appear to behave more or less like spherical objects whose diameters are the length of the monomer.

DOI: 10.1021/acsearthspacechem.8b00172
ACS Earth Space Chem. 2019, 3, 380−389

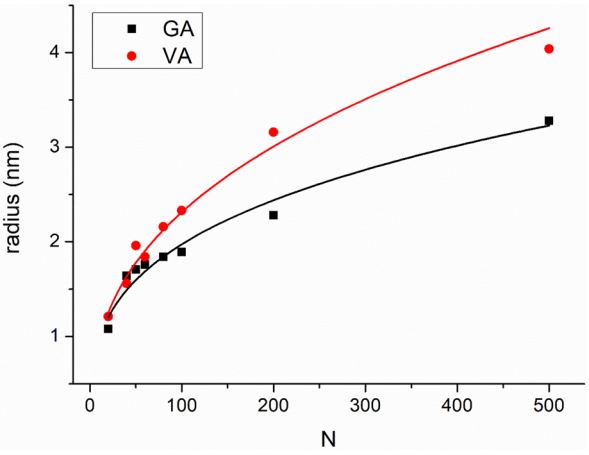

Figure 5. Comparison of the mean radius of the formed (black) GA or (red) VA particles as a function of the number N of molecules. The curves correspond to a $r(N) = r_0N^{\alpha}$ fit.

The density can be calculated from the number of molecules (N = 500) divided by the volume deduced from the Connolly surface (see Table 1). For GA, it is 1.04 g/cm^3, which is about 40% lower than the value measured at 298 K (1.41 g/cm^3[43]) for a solid bulk. For VA, the density is calculated to be 0.73 g/cm^3, which is about 20% less than the measured value of 0.93 g/cm^3.[44] Consistently, the model particles are much less dense than their corresponding bulk counterparts.

From the radii and estimated densities, we observe that VA aerosols are slightly less compact than the GA aerosols. This can be rationalized by the fact that one GA molecule has two acidic tails, instead of one acidic tail for VA. This allows for the formation of a larger number of hydrogen bonds per molecule on average and, thus, a more condensed aerosol.

Upon the addition of water on GA, the radius increases only slightly: for N = 500, by about 6% for the 1:1 acid/water ratio and 24% for the 1:2 acid/water ratio compared to the dry counterpart. The density for both wet aerosols is only slightly lower than that for the dry case (1.02 g/cm^3). Thus, the increase of mass due to water is compensated by the augmentation of the radius and, hence, the volume, indicating an inhomogeneous distribution of the molecules in the aggregate as observed on the RDFs (Figure 5).

Connolly Surfaces. Characterizing the surface in terms of the density of atoms gives some indication on the heterogeneous reactions that may occur depending upon the nature of the gaseous species impinging the particle. Figure 6 displays the surface repartition of the GA atoms for increasing aggregate sizes. Growing from 20 to 500 molecules only make the results vary by a few percentages, suggesting that the surface of relatively small particles could be representative of larger particles. Most of the surface is occupied by hydrogen atoms from the carbon chain (H_α and H_β), followed by both oxygen atoms from the acid functions. Acid functions represent about 40% of the surface, which explains why water is easily adsorbed on the aerosol. However, very few acidic hydrogen atoms are present at the surface, because they are involved in strong intermolecular bonds favoring the cohesion of the aerosol. The same trends occur for VA (not shown here) but with the hydrogen atoms from the methyl group being predominant (almost 50% of the total surface).

On Figure 7, the same distributions obtained for both 1:1 and 1:2 GA/water ratios are compared to the dry case for a

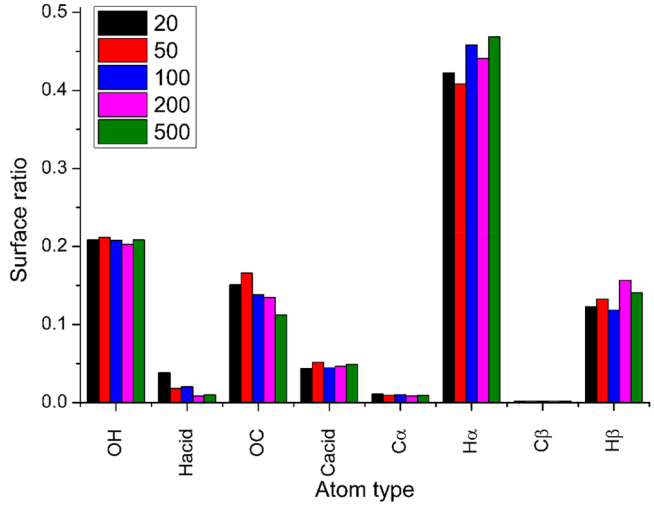

Figure 6. Atom distribution at the surface of dry GA particles for sizes varying between 20 and 500 molecules. The labels are described in Figure 1.

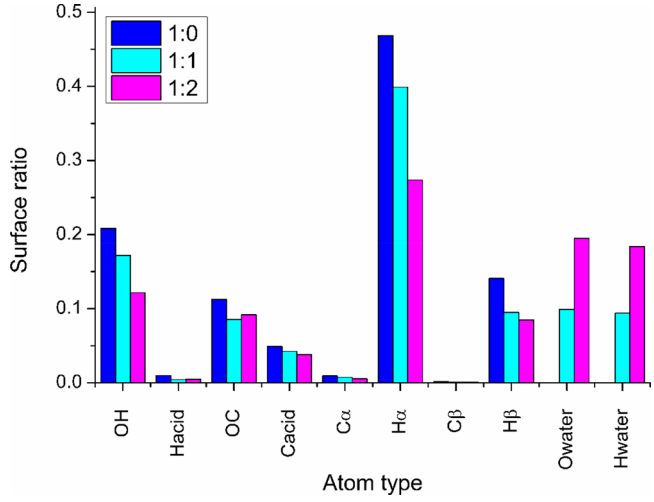

Figure 7. Comparison of the atom surface distribution of dry GA and both 1:1 and 1:2 ratios of GA/water aggregates containing 500 GA molecules.

500 molecule size. For the 1:1 ratio, about 20% of the surface is covered by water, while this proportion increases to about 40% for the 1:2 ratio. This is in agreement with the observation that water molecules tend to stay at the surface, according to the RDF depicted in Figure 4. Reciprocally, the amount of GA atoms remaining at the surface decreases. However, the relative proportion of each GA atom type does not change significantly with respect to the dry case. This further confirms that water molecules, even if adsorbed at the surface, do not induce any substantial change in the molecular organization. Finally, using the Connolly method, the water surface to bulk ratio is found to be 45% for the 1:1 case and 49% for the 1:2 case.

Hydrogen Bonds. The hydrogen bond length and O−O−H angle distribution for increasing sizes of GA and VA aggregates are shown in Figure 8. It should be recalled that, within our classical description, a strong hydrogen bond is characterized by a H−O bond of the order of 0.28−0.29 nm and a O···O−H angle close to 0°. For both molecules, the bond lengths are centered at the same value (~0.269 nm, Figure 8a for GA; 0.285 nm, Figure 8c for VA). These values

DOI: 10.1021/acsearthspacechem.8b00172
ACS Earth Space Chem. 2019, 3, 380−389

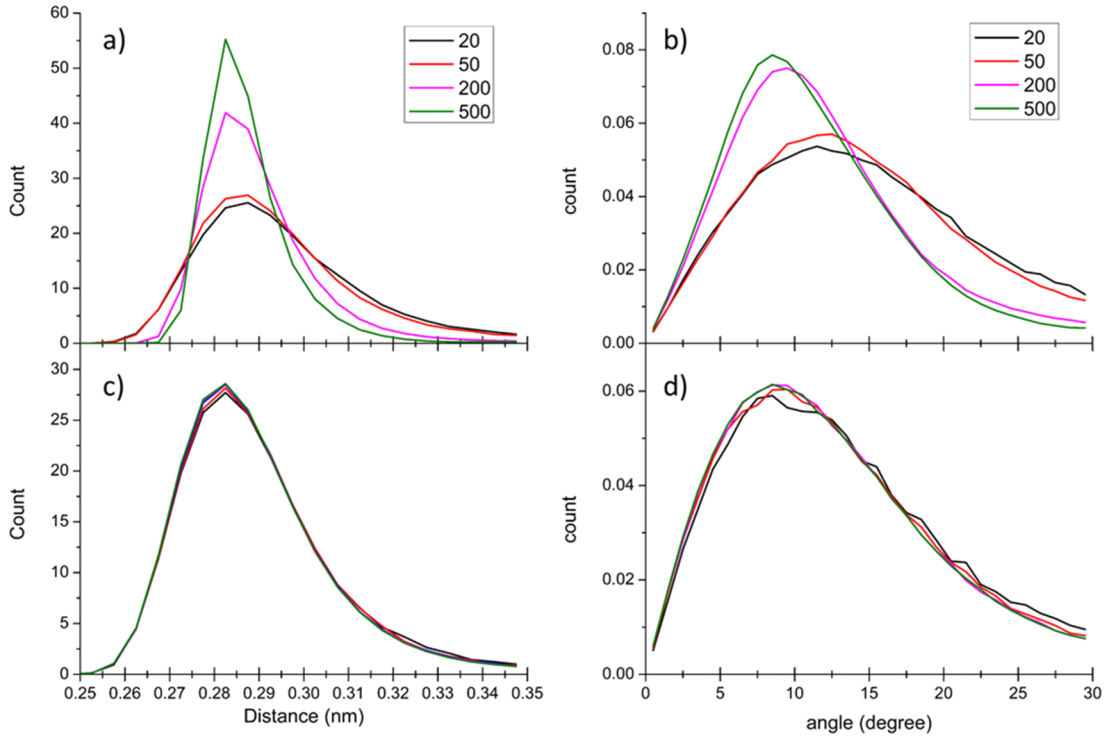

Figure 8. (a and c) Hydrogen bond distance distribution and (b and d) O···O−H angle distribution of dry (a and b) GA and (c and d) VA aerosols for sizes varying between 20 and 500 molecules.

are close to the experimental values.[39,40] As expected, the number of hydrogen bonds is about twice larger for GA than for VA. For VA, the distribution does not depend upon the size, while for GA, it becomes thinner as the number of molecules increases: the full width at half maximum (fwhm) decreases from ∼0.03 nm for N = 20 to ∼0.02 nm for N = 500. Similarly, it remains essentially constant around 10° for the angles (panels b and d of Figure 8), with the exception of a small shift when the GA aerosol size increases, meaning that the three atoms are almost perfectly colinear (Figure 8b). This angle is close to ∼12° found experimentally for both acids in the crystalline phase.[45,46] These results indicate that the core of the aggregate does not evolve during the growth for VA, whereas in the case of GA, the growth of the particle is associated with a significant strengthening of the hydrogen bonds. When water is added on GA (see the Supporting Information), the results remain essentially the same, for both acid/water ratios, supporting the previously stated assessment that water does not significantly change the molecular organization of the particle.

Complementary to the geometrical parameters, the dynamics of hydrogen bond formation/breaking inside the simulated aggregate can be characterized through the calculation of the time evolution of the hydrogen bond autocorrelation functions $a(t)$.[47] This is depicted in Figure 9 for small and large dry GA and VA aggregates. For both acids, the decay is faster for the small aggregate, indicating that the hydrogen bond lifetime is shorter. In comparison of the two acids, GA exhibits a slower decay than VA for each size and $a(t)$ is close to 1 and remains constant over time for N = 500. These trends are the signature of the difference of nature between the two acids: GA behaves like a solid, with the molecules being more tightly bonded, while VA behaves like a liquid. When water is added to GA,

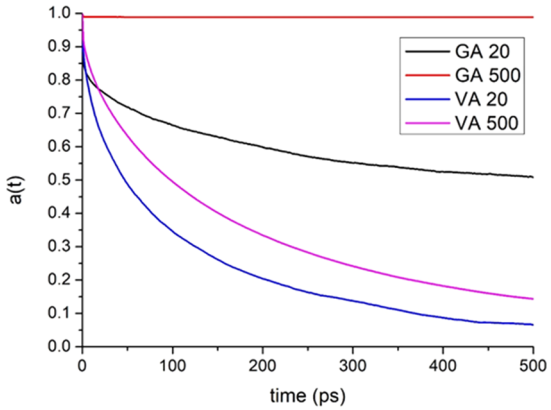

Figure 9. Autocorrelation function over hydrogen bonds between dry GA and VA aggregates of 20 and 500 molecules.

$a(t)$ remains the same and close to 1 for N = 500; therefore, the nature of the wetted aggregate is not significantly altered.

Binding Energies. With the water SPC/E model, a typical energy for a hydrogen bond formation is about 20 kJ/mol (e.g., see ref 48). For the acid−acid interaction, Darvas et al.[13] have implicitly assumed the same value for malonic−malonic acid and water−malonic acid interactions. The present simulations give a value of 90 kJ/mol for GA−GA, corresponding to four bonds, so that a typical value would be about 22.5 kJ/mol (see the Supporting Information). This is slightly below a previous MD value obtained on the crystal (27.4 kJ/mol in ref 49) but underestimated when compared to more refined results. Indeed, at the MP2/6-311++G(2d,2p)+ZPE level, we obtain for the gas-phase GA−GA dimer a value of 139 kJ/mol, corresponding to 34.7 kJ/mol per bond. This is close to the formic acid dimer, for which the best *ab initio* result (at MP2/VQZ2PP//TZ2P with counterpoise correction) is 31 kJ/

DOI: 10.1021/acsearthspacechem.8b00172
ACS Earth Space Chem. 2019, 3, 380−389

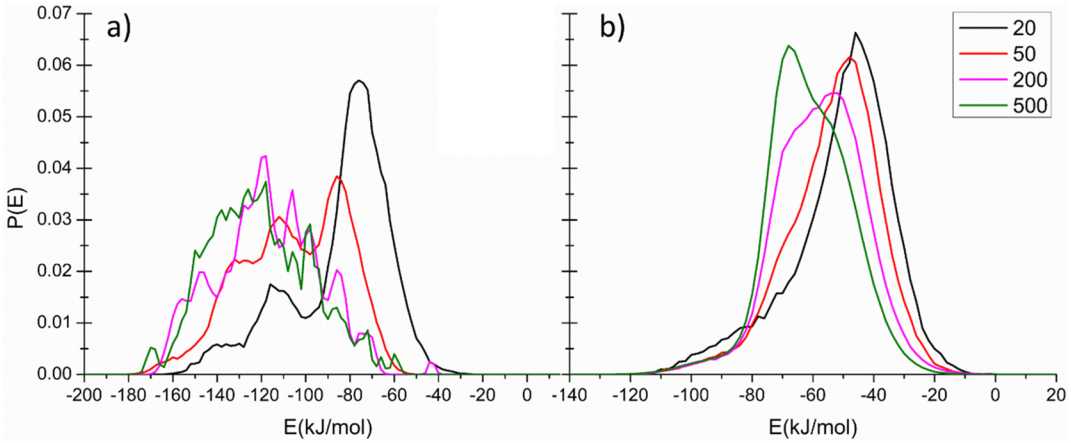

Figure 10. Binding energy distribution of dry (a) GA and (b) VA particles for 20−500 molecules.

mol.[50] In another work by Petit et al.[51] on C_6−C_{12} diacid crystals using density functional theory (DFT), an upper estimate of 42 kJ/mol per bond was obtained. As shown in the Supporting Information, the four bonds are not identical in their geometry, so that the energy of each of them is not strictly speaking the same. For the VA−VA dimer, the geometry of the dimer is simple because the two COOH groups form two very similar bonds (see the Supporting Information). The calculated MD energy of 29.3 kJ/mol (per bond) is very close to the MP2/6-311++G(2d,2p)+ZPE energy (31.5 kJ/mol) and just above classical simulations on the crystal (27.9 kJ/mol in ref 49). Finally, for the GA−water interaction, we use the "unfolded" isomer of the acid, more representative of what happens in the aggregate. The MD energy of the hydrogen bond is 42.7 kJ/mol, much larger than the *ab initio* result (28.5 kJ/mol). The same situation occurs for the VA−water case, because the MD value is 42.5 kJ/mol, while the *ab initio* result is 33.2 kJ/mol. Clearly, a more detailed study at the quantum level is needed, including basis set superposition error in particular, especially for the GA−GA and GA−water cases, but this is beyond the scope of the present study.

For consistency, the MD values will be used to obtain an estimation of the average number of hydrogen bonds per molecule in the analysis of the binding energy distributions of the aggregates. Such global distributions for dry GA and VA are depicted in Figure 10. For the smallest (N = 20; Figure 10b) VA cluster, the maximum is found around −40 kJ/mol, indicating between 1 or 2 hydrogen bonds. When the size increases, the maximum is shifted toward lower values, culminating to about −70 kJ/mol, i.e., between 2 and 3 bonds. The widths of the distributions are approximately the same. For GA (Figure 10a), the behavior is somewhat different qualitatively and quantitatively. For N = 20, there are well-defined peaks at about −80, −120, and −140 kJ/mol, characteristic of about 4, 5, and 6 bonds, respectively. The peak corresponding to the lowest number of bonds is by far the most intense. Increasing the size of the aggregate to 50 then 100 lowers the intensity of this first peak to the benefit of the second and third peaks. For even larger sizes, the peaks become less well-defined and the −80 kJ/mol peak disappears. For N = 500, the maximum probabilities now correspond to −120 and −140 kJ/mol and to a less extent −100 kJ/mol. This means that the number of hydrogen bonds is now about 6 ± 1. As expected from the dicarboxylic nature of GA, this number is roughly twice that found for VA and is consistent with the more compact nature of GA aggregates with respect to VA inferred from the density and hydrogen bond geometrical distributions.

When water is added, a more refined analysis is needed as a result of the three different types of interactions. Moreover, it is possible to distinguish between an acid molecule surrounded by water (GA−water) and a water molecule interacting with the surrounded acid molecules (water−GA). The binding energy distributions for 1:1 and 1:2 GA/water are displayed in Figure 11. The acid−acid binding distribution is compared to the dry case (Figure 11a). Upon the addition of water, the distribution is shifted toward higher energies, with the maximum being displaced from −120 kJ/mol in the dry case to −100 kJ/mol. This can be rationalized by the fact that some of the GA−GA bonds present in the dry aggregate have been broken in favor of interactions with water. This is clearly seen on the GA−water interaction (Figure 11b) that is characterized for both ratios by a broad distribution ranging between −100 and 0 kJ/mol. Dependent upon the configuration of the molecules in the aggregate and using the MD energy of 42.7 kJ/mol, the number of hydrogen bonds formed between one GA and water would then vary between 2 and 0. From the water point of view, the binding energy distributions are presented in Figure 11c, which gives the probability for a water molecule to be bonded to a GA molecule. For the 1:1 case, the maximum is indeed located around −40 kJ/mol, corresponding to 1 bond. At a ratio of 1:2, the distribution shape is slightly changed, with a larger proportion of water molecules that are not interacting with the carboxylic acids but that are instead interacting with other water molecules, as seen on the water−water binding energy distribution (Figure 11d), whose maximum is shifted toward lower energies as the number of water molecules increases. The binding energy analysis is representative of the formation of water islands at the surface of the organic aggregate.

These findings may be compared to two previous studies on similar systems, both with classical MD. First, Radola et al.[15] studied the formation of acetic and propionic acid aggregates for 1:1 to 1:6 water/acid ratios. The number of molecules was set to 120, but similar results were obtained with 240 molecules. Because of the use of the TIP5P potential for water,[52] the maximum temperature is 250 K and the typical water−water binding energy is about −25 kJ/mol. The results of the 1:1 propionic acid/water cluster at 250 K may be

DOI: 10.1021/acsearthspacechem.8b00172
ACS Earth Space Chem. 2019, 3, 380−389

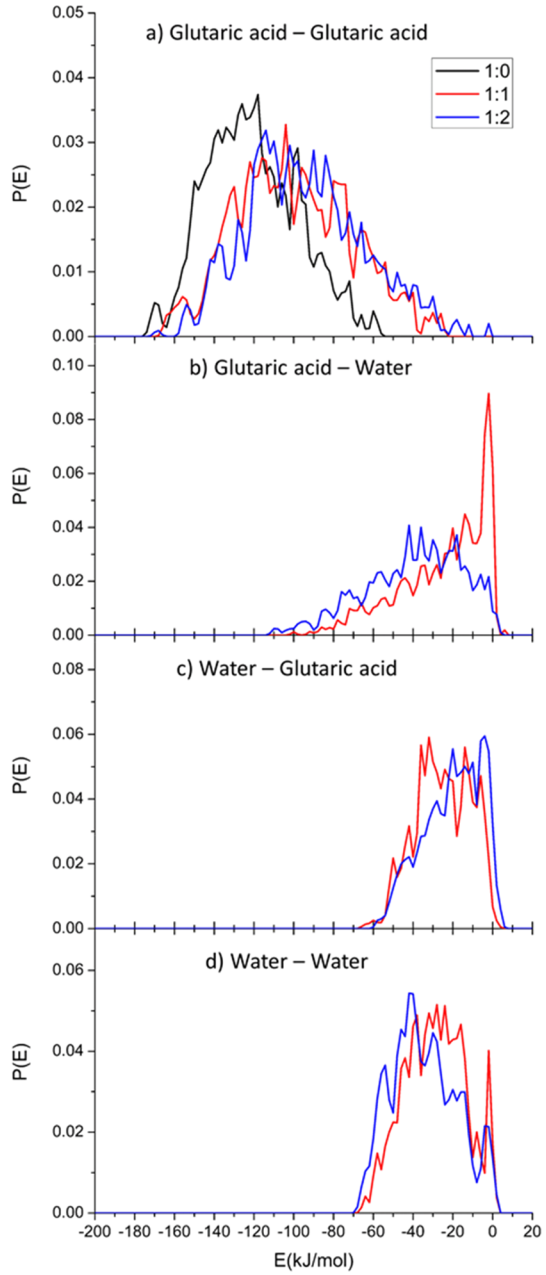

Figure 11. Comparison of binding energy distributions of dry (black) GA particles and (red) 1:1 and (blue) 1:2 GA/water particles for the (a) GA–GA, (b) GA–water, (c) water–GA, and (d) water–water interactions.

compared to the present 1:2 GA/water aggregate at 300 K. The three propionic–propionic, propionic–water, and water–water interactions show three well-defined peaks centered at −25, −25, and −75 kJ/mol. It should be kept in mind that these authors assumed the same value of −25 kJ/mol for all types of hydrogen bonds. Thus, at low water contents and high temperature, the results are similar to those for GA, with water islands scattered at the surface of the aggregate. However, because propionic acid is a monocarboxylic acid, the number of bonds is lower than that for GA. In another work,[13] Darvas et al. also used the same methods to study water adsorption on malonic acid aggregates, a smaller dicarboxylic acid ($C_3H_4O_4$). The use of 212 malonic acid molecules and 300 water molecules provides a ratio close to the present 1:2 GA/water ratio. As seen by comparison of Figure 5 of ref 13 to the present Figure 11, similar trends are observed: a broad distribution from malonic–malonic binding energy centered around −125 kJ/mol, three well-defined peaks at 0, −75, and −125 kJ/mol for malonic–water, and four peaks characteristic of 0–4 hydrogen bonds for water–water interactions. The competition between the acid–acid and acid–water interactions has also been observed for palmitic acid adsorbed on NaCl at various humidities.[53] For long-chain acids, lateral intermolecular interactions are also playing a role in the organization of the molecules and not only the bonding through the COOH groups.

CONCLUSION

MD simulations have been performed to model the formation of sub-micrometer organic aerosols of carboxylic acids, a monoacid (VA) and a diacid (GA), under dry or humid conditions at two acid/water ratios and ambient temperature. Two sets of comparisons have been addressed: first, GA aggregation properties have been compared to those of VA, and second, the alteration of the GA particle upon the addition of water has been studied.

The ability of GA to form hydrogen bonds on both sides of the chain triggers some significant differences in terms of structure, density, and binding energies with respect to VA. The aerosols composed of the diacid molecules are more compact than the monoacid molecules as a result of stronger intermolecular interactions. This is mostly due to the formation of a larger number of intermolecular hydrogen bonds that persist for a long time, even at room temperature.

When water is added on the particle, for a 1:1 acid/water ratio, it may be found in the core of small particles ($N < 100$); however, as the aggregate becomes larger, water tends to accumulate on the surface, forming aqueous islands on the organic particles. At higher humidity (1:2 ratio) and larger sizes ($100 < N < 500$), water molecules at the surface become pushed toward the center, forming an inhomogeneous particle containing water in the bulk and at the surface. This organization is driven by diffusion, and we can wonder if water will be able to completely diffuse toward the bulk, repelling the diacids toward the edge of the particle. Our simulations, even though extended to 90 ns, were not able to reach this state.

Interestingly, the atom distribution at the surface does not depend upon the size of the particle and is not significantly altered upon the addition of water, indicating that some substantial reorganization may only occur locally. This result provides confidence in the description of sub-micrometer particles with a limited number of molecules, although larger than 50 to obtain a significant surface/volume ratio. Descriptions of the organic aerosol surface and bulk at the molecular level can be of interest for laboratory experimentalists investigating the uptake or reactivity of trace gases on aerosol surfaces. Contrasting macroscopic measurements of elementary parameters (e.g., uptake coefficients of trace gases) obtained when environmental parameters are varied (e.g., RH and temperature) with changes in the aerosol surface composition simulated at the molecular level could help interpret experimental observations in more detail.

To study the uptake process of a radical or molecule at the particle surface and the potential reactions that could occur at the surface or within the bulk, approaches combining quantum chemistry and molecular mechanics have to be employed

DOI: 10.1021/acsearthspacechem.8b00172
ACS Earth Space Chem. 2019, 3, 380–389

(QM/MM). While these methods are becoming more and more efficient, the design of the system has, however, to satisfy the constraint of feasibility of the calculations and relevance of the chemical mechanisms. As such, our results give some indications on the atoms available at the surface and the representative particles that could be used for further investigation, including reactive processes.

■ ASSOCIATED CONTENT

Supporting Information

The Supporting Information is available free of charge on the ACS Publications website at DOI: 10.1021/acsearthspacechem.8b00172.

Force-field parameters, GA conformer distribution, crystal data, orientation distributions, and additional information on hydrogen bonding and surface contents for other acid/water ratios (PDF)

■ AUTHOR INFORMATION

Corresponding Author

*Telephone: +33-320434980. E-mail: denis.duflot@univ-lille.fr.

ORCID

Céline Toubin: 0000-0002-7379-8178
Sébastien Dusanter: 0000-0001-5162-3660
Véronique Riffault: 0000-0001-5572-0871
Denis Duflot: 0000-0002-8307-5344

Notes

The authors declare no competing financial interest.

■ ACKNOWLEDGMENTS

This work was performed using high-performance computing (HPC) resources from GENCI-TGCC (Grant 2018-A0010806820) and the Centre de Ressources Informatiques (CRI) of the University of Lille. The authors acknowledge support from the Chemical and Physical Properties of the Atmosphere (CaPPA) project, funded by the Agence Nationale de la Recherche (ANR) through the Programme d'Investissement d'Avenir (PIA) under Contract ANR-10-LABX-005 and contribution from the CPER research project CLIMIBIO. The authors also thank the French Ministère de l'Enseignement Supérieur et de la Recherche, the Hauts de France Region, and the European Funds for Regional Economic Development for their financial support. The authors thank Dr. J. Lovrić for helpful discussions.

■ REFERENCES

(1) Lazaridis, M. Organic Aerosols. In *Environmental Chemistry of Aerosols*; Colbeck, I, Ed.; Wiley-Blackwell: Hoboken, NJ, 2008; Chapter 4, pp 91−115; DOI: 10.1002/9781444305388.ch4.

(2) Paulot, F.; Paynter, D.; Ginoux, P.; Naik, V.; Horowitz, L. W. Changes in the aerosol direct radiative forcing from 2001 to 2015: Observational constraints and regional mechanisms. *Atmos. Chem. Phys.* **2018**, *18*, 13265−13281.

(3) Lohmann, U.; Feichter, J. Global indirect aerosol effects: A review. *Atmos. Chem. Phys.* **2005**, *5*, 715−737.

(4) Boreddy, S. K. R.; Kawamura, K.; Tachibana, E. Long-term (2001−2013) observations of water-soluble dicarboxylic acids and related compounds over the western North Pacific: Trends, seasonality and source apportionment. *Sci. Rep.* **2017**, *7*, 8518.

(5) Rozaini, M. Z. H. The Chemistry of Dicarboxylic Acids in the Atmospheric Aerosols. In *Atmospheric Aerosols—Regional Characteristics—Chemistry and Physics* Abdul-Razzak, H., Ed.; IntechOpen Limited: London, U.K., 2012; DOI: 10.5772/50127.

(6) Paulot, F.; Wunch, D.; Crounse, J. D.; Toon, G. C.; Millet, D. B.; DeCarlo, P. F.; Vigouroux, C.; Deutscher, N. M.; González Abad, G.; Notholt, J.; Warneke, T.; Hannigan, J. W.; Warneke, C.; de Gouw, J. A.; Dunlea, E. J.; De Mazière, M.; Griffith, D. W. T.; Bernath, P.; Jimenez, J. L.; Wennberg, P. O. Importance of secondary sources in the atmospheric budgets of formic and acetic acids. *Atmos. Chem. Phys.* **2011**, *11*, 1989−2013.

(7) Kawamura, K.; Bikkina, S. A review of dicarboxylic acids and related compounds in atmospheric aerosols: Molecular distributions, sources and transformation. *Atmos. Res.* **2016**, *170*, 140−160.

(8) Falkovich, A. H.; Graber, E. R.; Schkolnik, G.; Rudich, Y.; Maenhaut, W.; Artaxo, P. Low molecular weight organic acids in aerosol particles from Rondônia, Brazil, during the biomass-burning, transition and wet periods. *Atmos. Chem. Phys.* **2005**, *5*, 781−797.

(9) Mirivel, G.; Riffault, V.; Galloo, J.-C. Analysis of phthalic, isophthalic and long-chain (C_4−C_{12}) dicarboxylic acids in atmospheric aerosols by UPLC/ESI/ToF-MS. *Anal. Methods* **2011**, *3*, 1172.

(10) Crenn, V.; Fronval, I.; Petitprez, D.; Riffault, V. Fine particles sampled at an urban background site and an industrialized coastal site in Northern France — Part 1: Seasonal variations and chemical characterization. *Sci. Total Environ.* **2017**, *578*, 203−218.

(11) Ma, X.; Chakraborty, P.; Henz, B. J.; Zachariah, M. R. Molecular dynamic simulation of dicarboxylic acid coated aqueous aerosol: Structure and processing of water vapor. *Phys. Chem. Chem. Phys.* **2011**, *13*, 9374−9384.

(12) Darvas, M.; Picaud, S.; Jedlovszky, P. Water adsorption around oxalic acid aggregates: A molecular dynamics simulation of water nucleation on organic aerosols. *Phys. Chem. Chem. Phys.* **2011**, *13*, 19830−19839.

(13) Darvas, M.; Picaud, S.; Jedlovszky, P. Molecular dynamics simulations of the water adsorption around malonic acid aerosol models. *Phys. Chem. Chem. Phys.* **2013**, *15*, 10942−10951.

(14) Vardanega, D.; Picaud, S. Water and formic acid aggregates: A molecular dynamics study. *J. Chem. Phys.* **2014**, *141*, 104701.

(15) Radola, B.; Picaud, S.; Vardanega, D.; Jedlovszky, P. Molecular Dynamics Simulations of the Interaction between Water Molecules and Aggregates of Acetic or Propionic Acid Molecules. *J. Phys. Chem. B* **2015**, *119*, 15662−15674.

(16) Radola, B.; Picaud, S.; Vardanega, D.; Jedlovszky, P. Analysis of Mixed Formic and Acetic Acid Aggregates Interacting With Water: A Molecular Dynamics Simulation Study. *J. Phys. Chem. C* **2017**, *121*, 13863−13875.

(17) Taketani, F.; Kanaya, Y.; Akimoto, H. Kinetic Studies of Heterogeneous Reaction of HO_2 Radical by Dicarboxylic Acid Particles. *Int. J. Chem. Kinet.* **2013**, *45*, 560−565.

(18) Lakey, P. S. J.; George, I. J.; Whalley, L. K.; Baeza-Romero, M. T.; Heard, D. E. Measurements of the HO_2 Uptake Coefficients onto Single Component Organic Aerosols. *Environ. Sci. Technol.* **2015**, *49*, 4878−4885.

(19) Lakey, P. S. J.; Berkemeier, T.; Krapf, M.; Dommen, J.; Steimer, S. S.; Whalley, L. K.; Ingham, T.; Baeza-Romero, M. T.; Pöschl, U.; Shiraiwa, M.; Ammann, M.; Heard, D. E. The effect of viscosity and diffusion on the HO_2 uptake by sucrose and secondary organic aerosol particles. *Atmos. Chem. Phys.* **2016**, *16*, 13035−13047.

(20) Xu, W.; Zhang, R. Theoretical Investigation of Interaction of Dicarboxylic Acids with Common Aerosol Nucleation Precursors. *J. Phys. Chem. A* **2012**, *116*, 4539−4550.

(21) Abraham, M. J.; Murtola, T.; Schulz, R.; Páll, S.; Smith, J. C.; Hess, B.; Lindahl, E. GROMACS: High performance molecular simulations through multi-level parallelism from laptops to supercomputers. *SoftwareX* **2015**, *1−2*, 19−25.

(22) Zhao, Y.; Truhlar, D. G. The M06 suite of density functionals for main group thermochemistry, thermochemical kinetics, noncovalent interactions, excited states, and transition elements: Two new functionals and systematic testing of four M06-class functionals and 12 other functionals. *Theor. Chem. Acc.* **2008**, *120*, 215−241.

(23) Krishnan, R.; Binkley, J. S.; Seeger, R.; Pople, J. A. Self-consistent molecular orbital methods. XX. A basis set for correlated wave functions. *J. Chem. Phys.* **1980**, *72*, 650−654.
(24) Clark, T.; Chandrasekhar, J.; Spitznagel, G. W.; Schleyer, P. V. R. Efficient diffuse function-augmented basis sets for anion calculations. III. The 3-21+G basis set for first-row elements, Li−F. *J. Comput. Chem.* **1983**, *4*, 294−301.
(25) Frisch, M. J.; Trucks, G. W.; Schlegel, H. B.; Scuseria, G. E.; Robb, M. A.; Cheeseman, J. R.; Scalmani, G.; Barone, V.; Petersson, G. A.; Nakatsuji, H.; Li, X.; Caricato, M.; Marenich, A.; Bloino, J.; Janesko, B. G.; Gomperts, R.; Mennucci, B.; Hratchian, H. P.; Ortiz, J. V.; Izmaylov, A. F.; Sonnenberg, J. L.; Williams-Young, D.; Ding, F.; Lipparini, F.; Egidi, F.; Goings, J.; Peng, B.; Petrone, A.; Henderson, T.; Ranasinghe, D.; Zakrzewski, V. G.; Gao, J.; Rega, N.; Zheng, G.; Liang, W.; Hada, M.; Ehara, M.; Toyota, K.; Fukuda, R.; Hasegawa, J.; Ishida, M.; Nakajima, T.; Honda, Y.; Kitao, O.; Nakai, H.; Vreven, T.; Throssell, K.; Montgomery, J. A., Jr.; Peralta, J. E.; Ogliaro, F.; Bearpark, M.; Heyd, J. J.; Brothers, E.; Kudin, K. N.; Staroverov, V. N.; Keith, T.; Kobayashi, R.; Normand, J.; Raghavachari, K.; Rendell, A.; Burant, J. C.; Iyengar, S. S.; Tomasi, J.; Cossi, M.; Millam, J. M.; Klene, M.; Adamo, C.; Cammi, R.; Ochterski, J. W.; Martin, R. L.; Morokuma, K.; Farkas, Ö.; Foresman, J. B.; Fox, D. J. *Gaussian 16, Revision B.01*; Gaussian, Inc.: Wallingford, CT, 2016.
(26) Sousa da Silva, A. W.; Vranken, W. F. ACPYPE—AnteChamber PYthon Parser interfacE. *BMC Res. Notes* **2012**, *5*, 367.
(27) Wang, J.; Wolf, R. M.; Caldwell, J. W.; Kollman, P. A.; Case, D. A. Development and testing of a general amber force field. *J. Comput. Chem.* **2004**, *25*, 1157−1174.
(28) Bayly, C. I.; Cieplak, P.; Cornell, W.; Kollman, P. A. A well-behaved electrostatic potential based method using charge restraints for deriving atomic charges: The RESP model. *J. Phys. Chem.* **1993**, *97*, 10269−10280.
(29) Cieplak, P.; Cornell, W. D.; Bayly, C.; Kollman, P. A. Application of the multimolecule and multiconformational RESP methodology to biopolymers: Charge derivation for DNA, RNA, and proteins. *J. Comput. Chem.* **1995**, *16*, 1357−1377.
(30) Cornell, W. D.; Cieplak, P.; Bayly, C. I.; Kollman, P. A. Application of RESP charges to calculate conformational energies, hydrogen bond energies, and free energies of solvation. *J. Am. Chem. Soc.* **1993**, *115*, 9620−9631.
(31) Jakalian, A.; Jack, D. B.; Bayly, C. I. Fast, efficient generation of high-quality atomic charges. AM1-BCC model: II. Parameterization and validation. *J. Comput. Chem.* **2002**, *23*, 1623−1641.
(32) Berendsen, H. J. C.; Grigera, J. R.; Straatsma, T. P. The missing term in effective pair potentials. *J. Phys. Chem.* **1987**, *91*, 6269−6271.
(33) Bussi, G.; Donadio, D.; Parrinello, M. Canonical sampling through velocity rescaling. *J. Chem. Phys.* **2007**, *126*, No. 014101.
(34) Hess, B.; Bekker, H.; Berendsen, H. J. C.; Fraaije, J. G. E. M. LINCS: A linear constraint solver for molecular simulations. *J. Comput. Chem.* **1997**, *18*, 1463−1472.
(35) Darden, T.; York, D.; Pedersen, L. Particle mesh Ewald: An *N*·log(*N*) method for Ewald sums in large systems. *J. Chem. Phys.* **1993**, *98*, 10089−10092.
(36) Cochran, R. E.; Jayarathne, T.; Stone, E. A.; Grassian, V. H. Selectivity Across the Interface: A Test of Surface Activity in the Composition of Organic-Enriched Aerosols from Bubble Bursting. *J. Phys. Chem. Lett.* **2016**, *7*, 1692−1696.
(37) Connolly, M. Analytical molecular surface calculation. *J. Appl. Crystallogr.* **1983**, *16*, 548−558.
(38) Eisenhaber, F.; Lijnzaad, P.; Argos, P.; Sander, C.; Scharf, M. The double cubic lattice method: Efficient approaches to numerical integration of surface area and volume and to dot surface contouring of molecular assemblies. *J. Comput. Chem.* **1995**, *16*, 273−284.
(39) Scheuerman, R. F.; Sass, R. L. The crystal structure of valeric acid. *Acta Crystallogr.* **1962**, *15*, 1244−1247.
(40) Morrison, J. D.; Robertson, J. M. 212. The crystal and molecular structure of certain dicarboxylic acids. Part VII. *β*-Glutaric acid. *J. Chem. Soc.* **1949**, *0*, 1001−1008.
(41) Bhattacharya, S.; Saraswatula, V. G.; Saha, B. K. Thermal Expansion in Alkane Diacids—Another Property Showing Alternation in an Odd−Even Series. *Cryst. Growth Des.* **2013**, *13*, 3651−3656.
(42) Zhang, C.; Wang, Y.; Wang, H. Interaction between water and acetic acid-sodium halide aerosol: A molecular dynamics study. *Powder Technol.* **2017**, *314*, 9−19.
(43) Thalladi, V. R.; Nüsse, M.; Boese, R. The Melting Point Alternation in *α*,*ω*-Alkanedicarboxylic Acids. *J. Am. Chem. Soc.* **2000**, *122*, 9227−9236.
(44) Schill, G. P.; Tolbert, M. A. Depositional Ice Nucleation on Monocarboxylic Acids: Effect of the O:C Ratio. *J. Phys. Chem. A* **2012**, *116*, 6817−6822.
(45) Lifson, S.; Hagler, A. T.; Dauber, P. Consistent force field studies of intermolecular forces in hydrogen-bonded crystals. 1. Carboxylic acids, amides, and the C:O···H− hydrogen bonds. *J. Am. Chem. Soc.* **1979**, *101*, 5111−5121.
(46) Hagler, A. T.; Lifson, S.; Dauber, P. Consistent force field studies of intermolecular forces in hydrogen-bonded crystals. 2. A benchmark for the objective comparison of alternative force fields. *J. Am. Chem. Soc.* **1979**, *101*, 5122−5130.
(47) Rapaport, D. C. Hydrogen bonds in water. *Mol. Phys.* **1983**, *50*, 1151−1162.
(48) Zielkiewicz, J. Structural properties of water: Comparison of the SPC, SPCE, TIP4P, and TIP5P models of water. *J. Chem. Phys.* **2005**, *123*, 104501.
(49) Hagler, A. T.; Dauber, P.; Lifson, S. Consistent force field studies of intermolecular forces in hydrogen-bonded crystals. 3. The C:O···H−O hydrogen bond and the analysis of the energetics and packing of carboxylic acids. *J. Am. Chem. Soc.* **1979**, *101*, 5131−5141.
(50) Neuheuser, T.; Hess, B. A.; Reutel, C.; Weber, E. Ab Initio Calculations of Supramolecular Recognition Modes. Cyclic versus Noncyclic Hydrogen Bonding in the Formic Acid/Formamide System. *J. Phys. Chem.* **1994**, *98*, 6459−6467.
(51) Petit, L.; Lapalu, L.; Sautet, P. Self-Assembly of Diacid Molecules: A Theoretical Approach of Molecular Interactions. *J. Phys. Chem. C* **2009**, *113*, 17566−17571.
(52) Mahoney, M. W.; Jorgensen, W. L. A five-site model for liquid water and the reproduction of the density anomaly by rigid, nonpolarizable potential functions. *J. Chem. Phys.* **2000**, *112*, 8910−8922.
(53) Lovrić, J.; Duflot, D.; Monnerville, M.; Toubin, C.; Briquez, S. Water-Induced Organization of Palmitic Acid at the Surface of a Model Sea Salt Particle: A Molecular Dynamics Study. *J. Phys. Chem. A* **2016**, *120*, 10141−10149.

DOI: 10.1021/acsearthspacechem.8b00172
ACS Earth Space Chem. 2019, 3, 380−389